GLAUCOMA

Real-time intraocular pressure monitoring and responsive drug release in preclinical models by an all-polymer smart contact lens

Yuting Cai[1,2]†, Chenguang Zhang[3]†, Pengrui Dang[4], Chenshu Liu[1], Yuxuan Du[1], Reihaneh Haghniaz[1], Jiechen Wang[5], Safoora Khosravi[1,6], Zhengtang Luo[2], Peyman Servati[6], Lili Chen[3], James S. Wolffsohn[7], Tae-Woo Lee[8], Yangzhi Zhu[1]*

Glaucoma remains a leading cause of irreversible blindness worldwide, yet conventional topical therapies are often hampered by poor patient adherence, and standard in-office applanation tonometry captures only static measurements, failing to capture the dynamic nature of intraocular pressure (IOP). Smart contact lenses have emerged as promising tools for home-based, real-time IOP monitoring and feedback-guided therapy; however, most rely on bulky or rigid electronics that impair comfort, safety, and visual performance. Here, we report a battery-free, all-polymer microfluidic theranostic smart contact lens (AP-TSCL) that enables autonomous IOP-responsive glaucoma therapy without bulky electronic components. The AP-TSCL integrates a noninvasive microfluidic IOP sensor with a multistage, pressure-gated drug delivery architecture. Embedded microchannels define distinct activation thresholds, enabling lens deformation under elevated IOP to drive staged release from multiple drug reservoirs. Across in vitro (artificial eye model), ex vivo (enucleated bovine eyes), and in vivo (rabbit ocular hypertension) studies, the device achieved tonometry-aligned IOP tracking, pressure-triggered delivery of timolol or brimonidine above preset thresholds, and IOP lowering comparable to conventional topical therapy. This preclinical evidence suggests that the fully integrated platform may overcome key limitations of existing technologies and offers a clinically translatable solution for personalized ocular care.

INTRODUCTION

Glaucoma, often referred to as the "silent thief of sight," is the leading cause of irreversible blindness globally and the second leading cause in the United States. Driven largely by an aging population, its global prevalence is projected to rise sharply, from 80 million cases in 2020 to ~134 million by 2040 (*1*, *2*). As a chronic, progressive, and incurable disease, glaucoma requires early diagnosis, continuous monitoring, and sustained treatment to preserve vision and maintain quality of life (*3*). These clinical demands highlight the urgent need for effective theranostic technologies capable of identifying at-risk individuals, guiding personalized interventions, and reducing the burden on patients and health care systems.

Intraocular pressure (IOP) plays a central role in the pathogenesis and clinical management of glaucoma. Elevated IOP is the most prominent modifiable risk factor for both onset and progression, although individual susceptibility to IOP-induced optic nerve damage can vary widely (*4*, *5*). Lowering IOP remains the cornerstone of glaucoma therapy. Landmark studies such as the Ocular Hypertension Treatment Study (OHTS) and the Collaborative Normal Tension Glaucoma Study (CNTGS) demonstrated that IOP reductions of 20 to 30% can delay or halt disease progression (*6*–*8*). These findings form the basis for current clinical practice, which emphasizes personalized IOP-lowering targets based on baseline levels, optic nerve status, and disease severity, typically achieved through topical medications, laser therapy, or surgical interventions (*3*).

However, effective glaucoma management hinges on accurate and frequent IOP monitoring, an area where current clinical tools fall short. Goldmann applanation tonometry, the clinical standard, is performed only during infrequent office visits, typically 6 to 12 months apart, and provides a single–time-point snapshot that fails to capture the circadian and situational variability of IOP (*9*). IOP can fluctuate markedly because of factors such as body position, fluid intake, and time of day, particularly with peaks occurring in the early morning. This temporal variability can lead to underestimation or misclassification of disease risk and may result in inappropriate or suboptimal therapy. Therefore, there is an urgent need for more accessible, accurate, and continuous IOP monitoring tools that extend beyond the clinic.

Handheld tonometers such as the iCare Home provide an at-home alternative but are often cost-prohibitive to most patients (*10*). Electronic smart contact lenses (SCLs), such as the Sensimed TriggerFish, have been developed to enable continuous IOP monitoring; however, their reliance on rigid electronics and external power supplies has been reported to cause foreign body sensation, eye pain, superficial punctate keratitis, and corneal epithelial defects, limiting their practical use (*11*). These challenges highlight the need for a more affordable and comfortable solution for at-home IOP assessment.

[1]Terasaki Institute for Biomedical Innovation, Los Angeles, CA 91367, USA. [2]Department of Chemical and Biological Engineering, William Mong Institute of Nano Science and Technology, Hong Kong University of Science and Technology, Clear Water Bay, Kowloon 999077, Hong Kong, China. [3]Hospital of Stomatology, Guanghua School of Stomatology, Sun Yat-sen University, Guangdong Provincial Key Laboratory of Stomatology, Guangzhou 510055, China. [4]VIP Department, School and Hospital of Stomatology, China Medical University, Liaoning Provincial Key Laboratory of Oral Diseases, Shenyang, Liaoning 110002, China. [5]Department of Stomatology, Union Hospital, Tongji Medical College, Huazhong University of Science and Technology, Wuhan 430022, China. [6]Flexible Electronics and Energy Lab (FEEL), Department of Electrical and Computer Engineering, University of British Columbia, Vancouver, BC V6T 1Z4, Canada. [7]School of Optometry, College of Health and Life Sciences, Aston University, Birmingham B4 7ET, UK. [8]Department of Materials Science and Engineering, Institute of Engineering Research, Research Institute of Advanced Materials, Soft Foundry, Interdisciplinary Program in Bioengineering, Seoul National University, Seoul 08826, Republic of Korea.
†These authors contributed equally to this work.
*Corresponding author. Email: yzhu@terasaki.org

Topical IOP-lowering eye drops remain the first-line treatment for glaucoma but are limited by low bioavailability (less than 5% of the administered dose reaches intraocular tissues) (*12*) and a high incidence of local and systemic effects, ranging from ocular irritation to cardiovascular and respiratory complications (*13*). Moreover, long-term adherence is a major challenge: Compliance drops to ~40% within a year of treatment initiation (*14*) and is even lower among patients prescribed multiple medications (*15*). Poor adherence has been directly associated with worse visual outcomes, even when in-office IOP readings appear in the target range (*16*). Contributing factors include dosing complexity, side effects, forgetfulness, and financial burden. In addition, the reliance on periodic clinic visits for monitoring treatment efficacy introduces further barriers, particularly for patients in rural or underserved areas or during times of health care disruption, such as global pandemics. Although recent advances in sustained-release drug delivery systems, such as intracameral prostaglandin analog implants, have introduced new treatment paradigms, adoption remains limited. Concerns over corneal edema, endothelial toxicity, and implant dislodgement hinder repeat use and limit broader clinical integration. Despite these innovations, topical eye drops remain the standard of care, highlighting a critical unmet need for safe, effective, and user-friendly drug delivery systems in glaucoma.

SCLs represent a promising platform for integrating real-time IOP monitoring and feedback-controlled drug delivery into a closed-loop therapeutic system (*10*, *17*–*19*). However, their practical translation has been impeded by the need for embedded electronics, power sources, and associated manufacturing costs, all of which impair user comfort and limit accessibility. To address these challenges, we developed an all-polymer theranostic smart contact lens (AP-TSCL) capable of continuous IOP monitoring and autonomous programmable drug delivery without the need for bulky electronic components or manual operation. The AP-TSCL integrates a noninvasive, real-time microfluidic IOP sensor with a multidose, feedback-responsive drug release unit. A biomimetic mechanoactive and antiswelling silk sponge (BASS) enhances both sensing sensitivity and drug delivery consistency, yielding high mechanical robustness and excellent linearity across a physiological IOP range (16 to 32 mmHg). Comprehensive in vitro, ex vivo, and in vivo studies validate the AP-TSCL's biocompatibility, accuracy, and therapeutic efficacy, demonstrating its potential as a low-cost, patient-compliant platform for personalized glaucoma therapy in real-world settings.

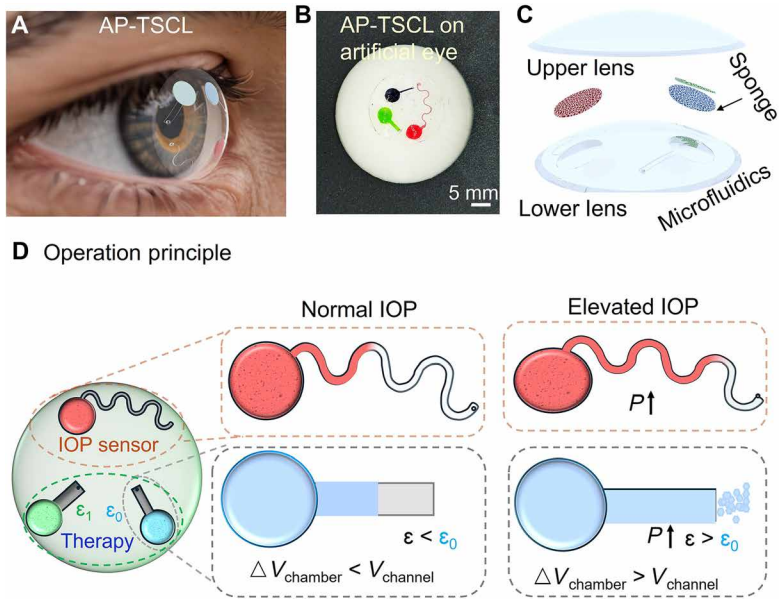

Fig. 1. Design of the AP-TSCL for real-time intraocular pressure monitoring and autonomous programmable therapy. (**A**) Use scenario showing a wearable, eye-conforming lens that integrates IOP sensing and drug delivery. (**B**) Photograph of the AP-TSCL on an artificial eye; black indicates the IOP-sensing unit, and blue/green indicates drug delivery reservoirs. (**C**) Schematic of the multilayer, sandwiched architecture enabling compact cointegration of sensing and delivery components. (**D**) Operating principle: Corneal deformation associated with IOP changes displaces a liquid interface for noninvasive IOP readout; elevated IOP reduces microchamber volume to actuate therapeutic release.

RESULTS

System design and working principle of the AP-TSCL

The AP-TSCL is designed to conform seamlessly to the corneal surface and to deform with changes in IOP (Fig. 1, A and B). This deformation translates corneal limbus expansion into a mechanical signal that can be detected by the integrated sensor, designed to enable real-time IOP readout and release of therapeutic agents directly onto the corneal surface. The AP-TSCL features a three-layered architecture: (i) a lower microfluidic lens layer containing microchannels and microchambers for both drug storage and IOP sensing; (ii) a middle BASS layer, which functions as both a strain-sensing component and drug reservoir; and (iii) an upper soft contact lens layer that encapsulates the device, mitigates blinking-induced mechanical pressure, and provides refractive correction (Fig. 1C).

To ensure structural integrity, we applied a precursor-bonded encapsulation technique developed in our previous work, forming covalent interfacial bonds between the upper and lower lens layers (fig. S1) (*20*). Here, we used a composite hydrogel consisting of poly(2-hydroxyethyl methacrylate)–silicone (polyHEMA-silicone) as the base material for fabricating the AP-TSCL. The material's surface wettability and chemical composition were characterized using contact angle measurements and Fourier transform infrared (FTIR) spectroscopy (figs. S2 and S3). The hydrophobic state corresponds to the as-fabricated (dry, nonhydrated) surface, whereas the hydrophilic state corresponds to the surface after hydration by soaking in artificial tears to equilibrium (fig. S2). We evaluated the bonding strength of the encapsulation layers, finding that dip-based encapsulation notably increased interfacial adhesion, with sequential dip coating followed by spray coating achieving the highest adhesion strength (~48 kPa) compared with physical contact (~13 kPa) and spray coating (~19 kPa) (fig. S4). The optical transmission of the lens was ~95% between 400- and 800-nm light range after encapsulation (fig. S5), a performance metric comparable to that of standard commercial soft contact lenses and essential for preserving patient visual acuity (*21*). Given hydrogel swelling upon hydration, potential changes in microchannel dimensions were assessed across the tested hydration range. No significant differences were observed in polyHEMA size change between immersion in water and the precursor solution ($P > 0.05$), supporting dimensional stability of the microchannels after encapsulation and assembly (fig. S6).

The dimensions of the AP-TSCL were tailored to match the anatomical contours of the human eye (*22*), using injection molding

techniques similar to those used for commercial contact lenses, with a base curve radius of 8.5 mm and a diameter of 16 mm (fig. S7). The design ensures conformal contact and mechanical stability, even under dynamic IOP fluctuations (*23*) (fig. S8). The fabrication and optimization of the AP-TSCL included iterative tuning of mold geometry and processing conditions to ensure reliable microchannel formation and alignment, as well as optimization of the encapsulation/bonding workflow to prevent leakage and delamination during hydration and handling (figs. S9 to S11). The IOP monitoring system comprises a sensing reservoir and a serpentine microchannel display, positioned near the lens periphery, well outside the visual axis, to avoid obstructing the user's field of vision (Fig. 1D, top). A serpentine microchannel was selected to enhance corneal conformability and mechanical durability by redistributing strain and minimizing stress concentrations during repeated IOP cycles, whereas its compact layout preserves optical transparency and the visual field in the limited lens area. The drug-loading reservoir, measuring 4 mm in diameter and 0.2 mm in height, was optimized to maximize storage capacity while maintaining a thin, compliant geometry for lens comfort. The microchannel display, with a width of 0.3 mm, was designed to minimize capillary artifacts because the Laplace pressure at the meniscus scales inversely with the characteristic hydraulic radius ($\Delta P^{cap} \approx 2\gamma\cos\theta/r^{eff}$) (*24*). Increasing the channel width reduces capillary rise, meniscus pinning, and unintended wicking (*25*), allowing the interface position to be governed primarily by IOP-driven volume displacement rather than by surface tension effects. This wider geometry also improves readability for direct visual inspection and smartphone imaging. The serpentine layout extends the sensing range while preserving mechanical flexibility, allowing the system to operate effectively within the compact geometry of a contact lens.

The on-demand drug delivery mechanism is activated by changes in the embedded microchamber volume, which are triggered by curvature alterations in both the cornea and the contact lens in response to variations in IOP. The microchannel functions as a conduit for the medication, delivering it to the corneal surface. When IOP-induced strain decreases the reservoir volume ($\triangle V_{chamber}$), the pressurized drug solution is forced through the microchannel. If $\triangle V_{chamber}$ remains smaller than the total volume of the microchannel ($V_{channel}$), the drug solution remains contained in the chamber and returns to the chamber when the IOP-induced strain subsides or is alleviated. Thus, a critical strain (ε_0) induced by an elevated IOP is required to initiate drug release. The threshold ε_0 is tunable by design, primarily through the geometry of the microchannel-chamber system and the mechanical properties of the deformable layer, including thickness and modulus, which together set the strain needed to transition from a closed to an open flow path. In this work, ε_0 was determined by correlating the onset of measurable release/meniscus displacement with the applied IOP (and corresponding strain) in calibrated benchtop tests (Fig. 1D, bottom), allowing the integrated drug delivery system to dynamically respond to fluctuations in the IOP profile. Furthermore, the necessity for personalized therapeutic regimes in glaucoma management calls for the development of a drug-eluting system capable of accommodating diverse drug types and individualized dosages. To meet this requirement, the AP-TSCL system has been designed to support programmable and combination delivery of multistage treatments, enabling tailored therapeutic strategies for each patient (fig. S12). A comparative summary of AP-TSCL and prior theranostic SCL platforms is provided (table S1).

Design and optimizations of the biomimetic mechanoactive silk sponge

Sea sponges, characterized by their hierarchical network of pores and microchannels, effectively regulate water intake and circulation, thereby optimizing the transport of nutrients, oxygen, and waste. Inspired by these natural systems and building on our previous research (*26*–*28*), we developed BASS structures for integration into an IOP monitor and on-demand therapeutic delivery system.

To optimize BASS properties, we investigated the influence of varying silk fibroin (SF) concentrations on the material porosity. The porous SF scaffold was fabricated using a lyophilization-based ice nucleation process to create an interconnected microporous network (fig. S13). Porosity decreased significantly as the SF concentration increased from 10 to 50 mg/ml, dropping from 60.8 to 37.9% ($P < 0.001$) (Fig. 2A). However, higher SF concentrations reduced the drug loading and retention capacity of the BASS (Fig. 2B). The three-dimensional porous networks of the BASS prepared at different SF concentrations exhibited distinct microstructures (fig. S14). Increasing the SF concentration produced a denser scaffold with reduced pore size and diminished pore interconnectivity, consistent with the measured decrease in porosity. Fluid absorption assessments revealed a reduced absorption capacity with increasing SF concentration; the 50-mg/ml group showed lower absorption than the 10-mg/ml group (19,266.6 and 37,333.3%, respectively; $P < 0.001$) (Fig. 2B), likely attributable to the decreased porosity and the resulting denser porous network. BASS fabricated with a 30-mg/ml SF solution demonstrated optimal performance, absorbing ~2700 times their original dry weight in a short time.

We further evaluated the mechanical stability and structural recovery of the BASS synthesized at different SF concentrations (Fig. 2C). BASS with SF concentrations above 30 mg/ml displayed rapid shape recovery and high recovery ratios after strain removal, even after 100 cycles, highlighting their robust elasticity due to the reversible porous structure. In addition, BASS fabricated with a 30-mg/ml SF solution maintained nearly 100% of its original liquid loading capacity after 100 consecutive compression cycles at strains ranging from 5 to 25% (Fig. 2D). After 100 successive compressions at different strains (5 to 25%), BASS (30 mg/ml SF) maintained elastic resilience (Fig. 2E). BASS exhibited antiswelling behavior and comparable loading capacity across different aqueous solutions (equal volume), including dye- and drug-containing formulations (Fig. 2F).

The drug-loading capacity of the BASS was further evaluated using a brimonidine tartrate aqueous solution (1 mg/ml). During a 3-hour incubation of drug-loaded BASS in the same loading solution, the bulk concentration remained unchanged, indicating minimal leaching under loading/holding conditions (fig. S15). In contrast, when transferred to deionized water (sink conditions), the loaded drug was rapidly released, with nearly 100% release, confirming efficient release upon medium exchange and minimal drug loss during integration/handling (fig. S16).

Benchtop evaluation for AI-assisted real-time IOP quantification

The IOP monitoring system comprises the BASS, a sensing reservoir, and a microchanneled display. The integration of the BASS plays a crucial role in maintaining the operational stability of the IOP sensor, addressing the critical challenge of microchannel collapse, which can lead to sensor malfunctions such as reduced sensitivity and unstable interface movement. To overcome this challenge,

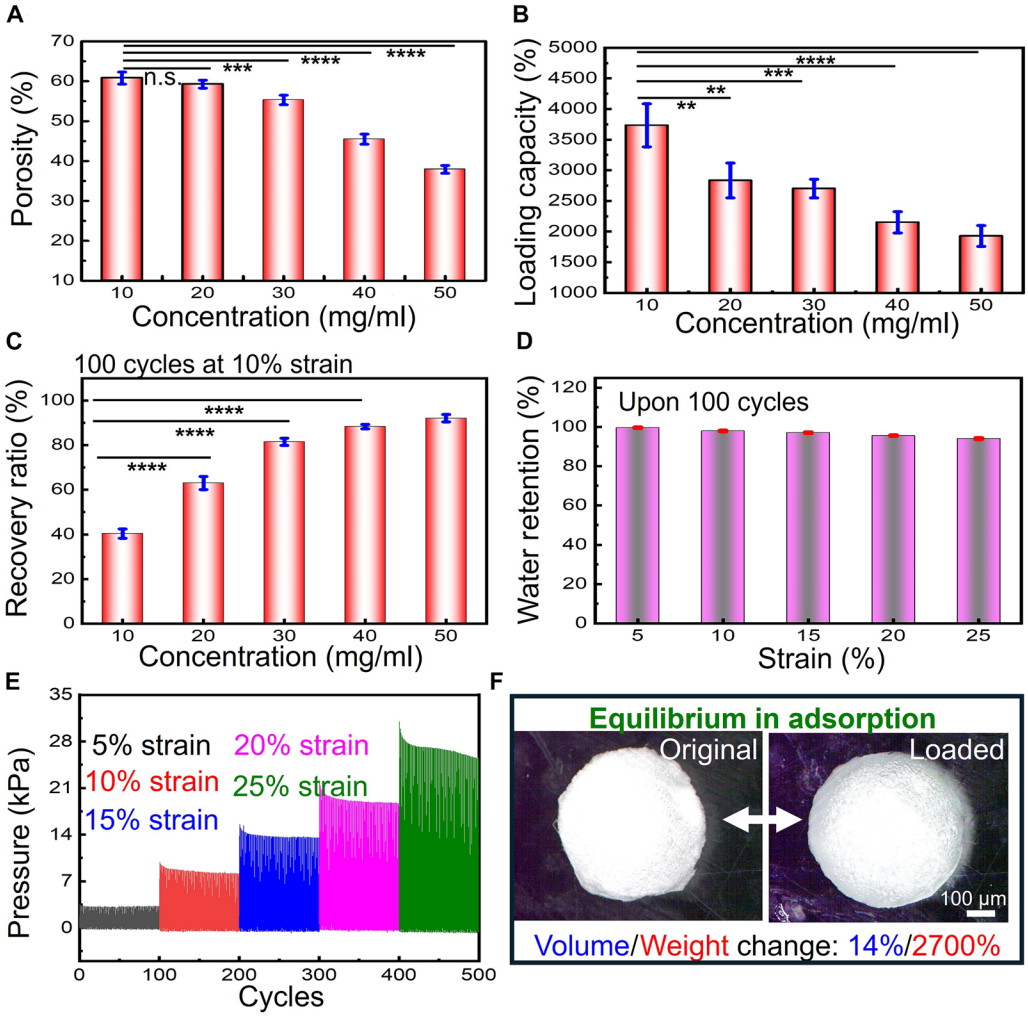

Fig. 2. Physicomechanical characterization of the BASS. (**A**) Porosity of the BASS fabricated with SF concentrations ranging from 10 to 50 mg/ml. (**B**) Liquid loading capacity of the BASS prepared with varying SF concentrations (10 to 50 mg/ml). (**C**) Water recovery ratio of the BASS after 100 compression cycles at 10% strain, showing that higher SF concentrations lead to an increased recovery ratio. (**D**) Water retention capacity of the BASS made from a 30-mg/ml SF solution after 100 compression cycles across strains ranging from 5 to 25%. (**E**) Mechanical fatigue performance of the BASS (30 mg/ml SF) under 100 compression cycles at strains ranging from 5 to 25%. (**F**) Photographs illustrating the change in volume and weight after complete hydration, with a maximum weight increase of 2700% while the volume change remains below 14%. Data are presented as means ± SD; $n = 3$. Statistical comparisons are indicated in the plot. For ≥3 groups, one-way ANOVA with Tukey's post hoc test was used; for two-group comparisons, unpaired two-tailed Welch's t tests were used. Significance is denoted by brackets between the compared groups (*$P < 0.05$, **$P < 0.01$, ***$P < 0.001$, and ****$P < 0.0001$; n.s., not significant).

the microchannel display was designed with a serpentine structure, ensuring flexibility and a broad working range in the limited lens area. To assess the safety and stability of the AP-TSCL, we used biocompatible dyed fish oil as the indicator liquid in the IOP display system. No detectable diffusion or leakage of the indicator liquid was observed over a 1-month period, confirming the long-term sealing integrity of the microfluidic reservoir (fig. S17).

The AP-TSCL allows visualization of IOP changes by detecting corneal deformation caused by IOP fluctuations and translating these deformations into measurable liquid displacements at the microchannel interface. When IOP increases, the corneal radius of curvature expands, prompting the sensing reservoir, supported by the BASS, to conform to the corneal shape because of the surface tension of the tear film. This deformation reduces the reservoir volume, displacing fluid into the microchannel display, correlating with the elevated IOP. As the IOP returns to its baseline range, the fluid flows back to the reservoir, demonstrating the monitor's reversibility (movie S1). The integration of the BASS improved mechanical robustness and sensing reliability, as supported by BASS fatigue/shape recovery and liquid retention under cyclic compression (Fig. 2, C to E) and by device-level sealing and operation stability under prolonged testing (figs. S17 and S24 and movie S1). In the absence of the BASS, void microstructures formed during fabrication, leading to collapse and deformation of both the microfluidic reservoir and the display microchannel, which, in turn, resulted in erroneous or unstable IOP readings (figs. S18 and S19). Although direct comparative testing between sensors with and without BASS was not feasible because of fabrication limitations, we performed a series of comprehensive in vitro assessments to validate the performance of the BASS-integrated AP-TSCL.

To replicate the ocular environment filled with tear fluids, we conducted an in vitro benchtop evaluation by affixing the AP-TSCL to an artificial eyeball in a reservoir filled with artificial tear fluids (fig. S20). The soft artificial eyeball, fabricated from polydimethylsiloxane (PDMS), was optimized for an elastic modulus similar to that of the human cornea/sclera complex (fig. S21). A manometer visualized the IOP, and a syringe pump generated pressure variations. The IOP was actively controlled by a syringe pump and increased stepwise from 16 to 40 mmHg in 3-mmHg increments (0.4 mmHg s^{-1}), whereas the sensor displacement was recorded at each pressure level (fig. S22). The sensor demonstrated high sensitivity, with a response of 0.14 mm/mmHg and an excellent linear relationship ($R^2 = 0.99$) in the range of 19 to 40 mmHg (fig. S23), important for identifying and tracking glaucoma staging and progression. This high linearity highlights the device's suitability for accurate and real-time IOP monitoring in both clinical and at-home settings. To evaluate dynamic sensing behavior, we conducted cyclic loading tests in which the IOP was varied between 15 and 31 mmHg over multiple cycles. The microchannel displacement exhibited highly reproducible responses, with robust synchronization across cycles, confirming the reversibility and repeatability of the sensor (fig. S24A). We further examined long-term stability by applying repeated pressure increments from 16 to 28 mmHg over a 7-day period. Displacement signals remained highly uniform across daily measurements, demonstrating the sensor's excellent operational stability for chronic IOP monitoring (fig. S24B).

Detecting subtle fluctuations in IOP with the naked eye is impractical. To address this limitation, we implemented a smartphone-enabled imaging system to capture microfluidic displacements and enable precise quantification of IOP fluctuations. This approach was validated in both benchtop tests and subsequent in vivo studies. To further improve automation and accuracy, we developed an AI-based computer vision model capable of real-time detection and interpretation of the microfluidic display response for IOP monitoring. This vision-based model automates the interpretation of fluid displacement in the embedded microchamber and directly outputs IOP estimations in numerical form (Fig. 3A). The system captures video input from a webcam and processes the live frames to track and quantify microfluidic behavior continuously, eliminating the need for manual frame-by-frame inspection (Fig. 3B and movie S2).

Once the region of interest (ROI) is defined to correspond with the microchannel display (Fig. 3C, i), the system activates a kernelized correlation filter (KCF) tracker, implemented in OpenCV, to maintain robust tracking of the chamber across subsequent frames (Fig. 3C, ii). After ROI selection, the red-enhanced display region undergoes processing through a convolutional neural network (CNN), which extracts spatial features and maps these visual characteristics to a numerical value representing the inferred IOP (Fig. 3, C, iii and D). This approach supports continuous and dynamic monitoring of IOP changes by updating predictions in real time across frames. To evaluate model performance, we conducted controlled experiments with recorded or live video data in which the true IOP was modulated over time. The CNN-predicted IOP values were compared against ground truth measurements, yielding a linear regression fit with a correlation coefficient of $r = 0.94$ (Fig. 3E). This strong correlation demonstrates that the model accurately captures both the trend and magnitude of IOP changes. The slight underestimation in slope and offset in intercept indicate a small, correctable bias, likely due to training set composition, and may be addressed through post hoc calibration. Overall, the system demonstrates the feasibility of using visual readouts of microfluidic behavior combined with real-time computer vision to estimate IOP continuously and noninvasively. By eliminating subjective interpretation and enhancing reproducibility, this automated pipeline offers a scalable solution for on-demand pressure monitoring using SCL platforms. Its deployment on accessible hardware (for example, smartphones) further supports clinical translation and user-friendly implementation. In addition, to enhance the practical usability of the AP-TSCL under low-light or dark conditions, the AP-TSCL reading module incorporates an adaptive illumination system that activates only when the eye is correctly aligned with the smartphone camera. This design enables accurate and consistent imaging of the microfluidic channels regardless of ambient lighting, thereby ensuring reliable IOP visualization in dim environments without interference from environmental light sources (figs. S25 and S26).

Assessment of autonomous IOP-responsive drug delivery

Our AP-TSCL system achieves autonomous drug delivery through a mechanoresponsive mechanism, not an electronically driven closed loop. Unlike smart lenses that use real-time sensors, signal processing, and actuators to adjust dosing in prior state-of-the-art designs, our design removes the need of external electronics: The drug reservoir itself serves as both sensor and actuator by deforming and releasing medication only when IOP exceeds a preset IOP threshold. Although the IOP monitoring module and drug release reservoir are cofabricated, they function independently; IOP readouts inform clinical assessment but do not digitally trigger release. The AP-TSCL delivers drug through passive, pressure-induced deformation of the integrated microchamber that mechanically opens the microfluidic flow path, coupling sensing and actuation without any electronic trigger. Such on-demand drug delivery function is activated by the deformation of its integrated microchamber in response to changes in corneal and contact lens curvature due to IOP variations. Wider microfluidic channels require higher IOP thresholds for medication release because of their increased volume (Fig. 4A). Specifically, a 0.5-mm microfluidic channel (highlighted in blue) releases medication at an IOP of 22 mmHg, a threshold associated with high glaucoma risk (*29*, *30*). The inset provides a magnified view of the 0.5-mm-wide microfluidic channel. The medication release process occurs as IOP increases from 16 to 22 mmHg and subsequently returns to 16 mmHg (fig. S27 and movie S3). Similarly, a 0.7-mm microfluidic channel releases medication at a higher IOP of 26 mmHg. AP-TSCLs with microfluidic widths of 0.5, 0.7, and 1 mm were tested to explore release profiles under elevated IOP conditions, simulating glaucoma progression (Fig. 4B). Unlike prior experiments using dye for optimizations, we used brimonidine, a US Food and Drug Administration (FDA)–approved antiglaucoma medication, to investigate the release profile. No release was observed until the specific IOP threshold (22, 26, and 32 mmHg) was achieved, indicating accurate release control. Subsequent experiments focused on AP-TSCL with 0.5-mm channels, corresponding to a 22-mmHg release threshold.

To validate the IOP-responsive behavior of the AP-TSCL, IOP was incrementally and cyclically increased from 16 to 22 mmHg. Drug release was consistently initiated only when the IOP reached the threshold (22 mmHg), confirming pressure-gated triggering (Fig. 4C). Cumulative drug releases increased progressively over 10 consecutive IOP modulation cycles (Fig. 4D and fig. S28). Pressure modulation triggered drug release in each cycle (fig. S29). The amount released per cycle decreased gradually over repeated cycles, consistent with

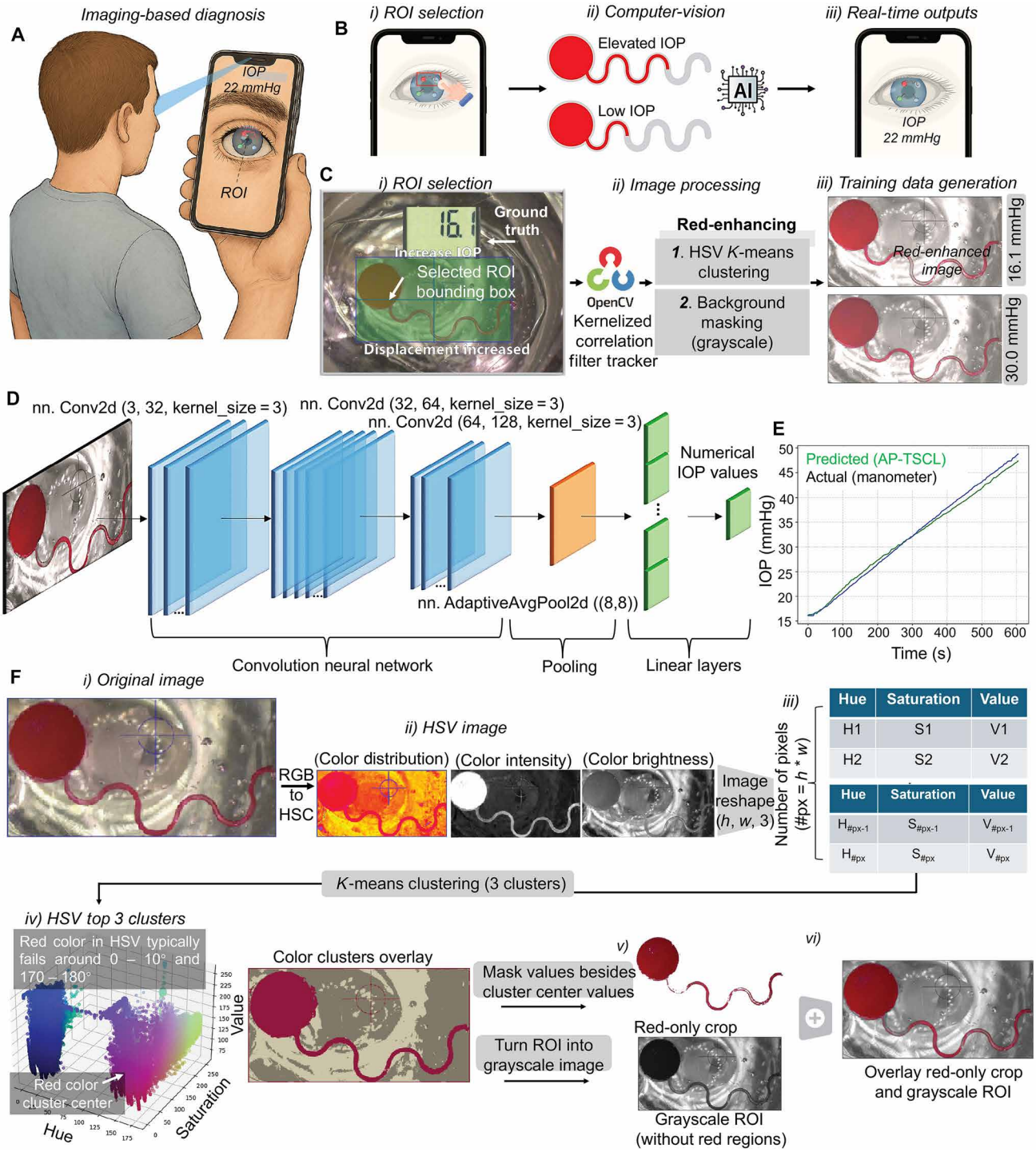

Fig. 3. Computer vision–based analytical pipeline for real-time IOP monitoring. (**A**) Schematic of a webcam-enabled vision system for real-time IOP tracking using a smartphone. The user wears the AP-TSCL and positions the eye in the camera field of view for continuous acquisition. (**B**) Real-time analysis workflow: (i) user-defined selection of the ROI corresponding to the microfluidic chamber, (ii) continuous ROI tracking across video frames using a trained vision algorithm, and (iii) frame-by-frame estimation of IOP based on fluid displacement in the microchannel. (**C**) Data acquisition and preprocessing pipeline for model training: (i) ROI tracking implemented using a KCF in OpenCV, (ii) color enhancement to emphasize red fluid motion, and (iii) pairing of processed images with corresponding labeled IOP values for supervised learning. (**D**) Schematic of the CNN architecture used for IOP inference, comprising three convolutional layers, one pooling layer, and two fully connected layers that output a single IOP value per frame. (**E**) Linear regression comparing CNN-predicted IOP with reference IOP measurements for model evaluation ($R^2 = 0.94$, $P < 0.001$; $n = 122$). (**F**) Image enhancement pipeline for microfluidic chamber visualization: (i) conversion from BGR to HSV color space, (ii to iv) *K*-means clustering to segment dominant color regions and isolate the red channel, and (v and vi) application of a binary mask to enhance the red fluid signal while rendering the background in grayscale to facilitate downstream analysis. Schematic illustrations created in OpenCV and Adobe Illustrator.

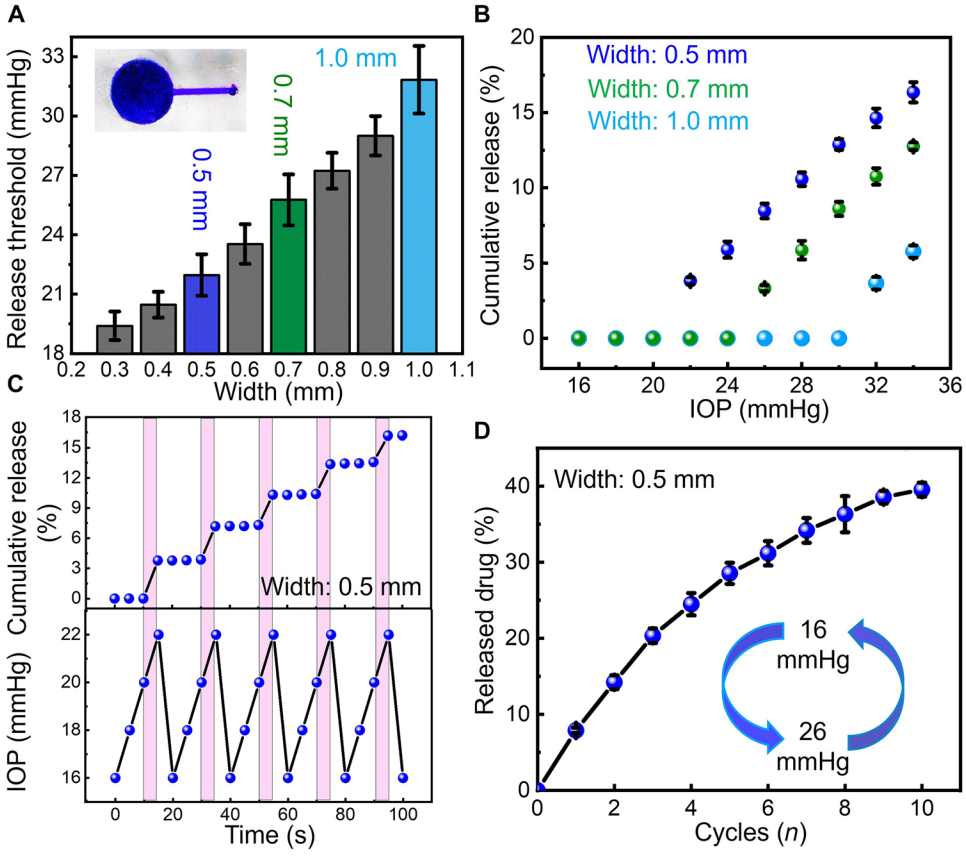

Fig. 4. Tuning IOP-responsive drug delivery through microfluidic design in the AP-TSCL. (**A**) Quantified IOP release threshold as a function of embedded microchannel width (0.3 to 1.0 mm), with representative examples shown for widths of 0.5, 0.7, and 1.0 mm; the inset shows a photograph of the 0.5-mm microfluidic channel. (**B**) Cumulative drug release profiles for three channel widths (0.5, 0.7, and 1.0 mm) across a physiologically relevant IOP range (16 to 36 mmHg). $n = 3$. Data are presented as means ± SD. (**C**) Example multistage release using the 0.5-mm channel during repeated IOP changes between 16 and 22 mmHg. (**D**) Cumulative release under repeated pressure cycles between 16 and 26 mmHg. Data are presented as means ± SD; dots represent individual replicates; $n = 3$ per condition.

progressive depletion of a finite reservoir during repeated triggering. Minimal or no release was observed below the critical IOP (~22 mmHg), followed by a steep rise in released volume as pressure increased above this threshold. This response profile reflects the designed functionality of the feedback-controlled microfluidic system, enabling drug administration primarily under pathologically elevated IOP conditions. A standard calibration curve was used to quantify timolol amounts in the release studies reported in this study (fig. S30).

Even under the highest tested IOP condition (30 mmHg), the total volume of drug released remained below 2.5 μl, corresponding to ~25 μg of 1% timolol, only 10% of the standard clinical dose (250 μg in a 50-μl drop of 0.5% timolol). At lower IOP values, the released amount remained negligible, thereby reinforcing the safety of the AP-TSCL platform by avoiding overtreatment and minimizing systemic exposure. The timolol dosage comparison between commercial eye drops and the AP-TSCL platform is provided in the Supplementary Materials (table S2). Controlled experiments were conducted to evaluate drug release from the AP-TSCL under varying IOP levels. Cumulative release followed a nonlinear pressure-dependent profile with an activation threshold near 22 mmHg; drug output was near zero below this pressure and measurable once it was exceeded (fig. S31). Release behavior under stepwise pressure application was used to assess drug release under sustained high-pressure conditions, where IOP was maintained at discrete levels for 1-hour intervals (fig. S32). Under static conditions, only minor diffusion-driven release was detected. However, each incremental increase in IOP led to a higher drug release event, indicating that the system is responsive to dynamic pressure changes rather than sustained load. These results confirm that the AP-TSCL enables mechanoresponsive, IOP-dependent drug delivery, selectively activated by fluctuations in IOP.

Moreover, we investigated the potential impact of blinking-induced mechanical pressure on unintended drug release as normal eyelid pressure typically remains below 7.5 mmHg (around 1 kPa) (*20*). An eye-blinking simulation setup was used to apply accurate eyelid pressure (*20*) (fig. S33A and movie S4). Minimal drug release occurred under 1 kPa at a frequency of 1.5 Hz, regardless of whether the pressure was applied horizontally or vertically (fig. S33B). This stability is attributed by several design features of the AP-TSCL: (i) The BASS component serves as a buffer, absorbing transient, rapid pressure changes such as those caused by blinking, which differ from the progressive IOP increases associated with glaucoma; (ii) the microfluidics are fully integrated into the base lens, directly in contact with the corneal surface and insulated by the top lens, further protecting the drug release module from eyelid pressure.

To ensure translational feasibility and device robustness in real-world applications, we systematically evaluated drug retention and mechanical reliability of the AP-TSCL under practical conditions. To mitigate drug loss because of passive diffusion during storage or wear, we applied a conformal, pinhole-free parylene coating to the inner surfaces of the microfluidic reservoirs. Parylene, known for its hydrophobicity and chemical inertness, forms an effective diffusion barrier for water-soluble drugs. The coating was uniformly deposited throughout the channel structures (fig. S34). To evaluate the potential for passive drug leakage during storage, particularly for water-soluble therapeutics such as timolol and brimonidine, we conducted extended leakage tests under clinically relevant conditions. AP-TSCL

devices were loaded with aqueous drug solutions and immersed in artificial tears at physiological temperature (35°C) (fig. S35). Devices without parylene coating exhibited obvious leakage, with >70% cumulative drug release observed over a 21-day period. In contrast, parylene-coated AP-TSCLs retained >95% of their initial drug content, confirming the critical role of the parylene barrier in minimizing long-term diffusion-based loss during storage and handling.

We also assessed the risk of unintentional drug release during lens application and removal. Manual handling simulations were performed using both artificial eyeballs and ex vivo bovine eyes. When finger pressure was applied exclusively to the peripheral (nondrug) region of the lens, no drug release was observed (fig. S36). The corresponding deformation was insufficient to exceed the critical volume threshold ($\Delta V_{chamber} > V_{channel}$) required to activate the release mechanism. Furthermore, the microfluidic drug reservoir and delivery channels are physically encapsulated between the upper and lower lens layers, forming an intrinsic mechanical buffer that dissipates incidental surface pressure and protects the functional core from direct compression.

In vitro analysis of an autonomous, programmable drug delivery system

Establishing personalized IOP-lowering goals on the basis of the maximum untreated IOP and individual disease severity is central to current glaucoma management paradigms. However, the addition of multiple medications often imposes financial and emotional burdens on patients, largely because of poor adherence and complex dosing schedules (*31*, *32*). These challenges hinder efforts to reduce the socioeconomic impact of glaucoma.

To address this unmet clinical need, we developed two distinct treatment configurations in a unified AP-TSCL platform: AP-TSCL-Timo, loaded with timolol for standard monotherapy, and AP-TSCL-Pro, coloaded with timolol and brimonidine for programmable, multistage therapy, each designed to support personalized glaucoma management. Clinical studies have shown that monotherapy, even with increased dosing frequency, is often insufficient for effective long-term IOP control (*33*). In this context, the AP-TSCL's ability to deliver multiple medications either simultaneously or in a programmable sequence represents a promising strategy to enhance therapeutic efficacy, reduce treatment burden, and improve patient adherence.

The design of the combination therapy included two identical microfluidic channels (0.5 mm in width) that are integrated into the AP-TSCL system (Fig. 5A), each loaded with a different medication, timolol and brimonidine, both of which are clinically approved IOP-lowering drugs (*34*, *35*). When IOP-induced strain reduces the microchamber volume change ($\triangle V_{chamber}$) beyond the volume of the microfluidic channel ($V_{channel}$), the drug solutions are pressurized and delivered to the corneal surface.

We observed simultaneous timolol and brimonidine release when IOP approaches around 22 mmHg, with output governed by pressure, enabling on-demand delivery upon IOP fluctuations (Fig. 5B). This effect was further confirmed by ultraviolet-visible (UV-Vis) spectrophotometric analysis (Fig. 5C). Timolol and brimonidine exhibit distinct maximal absorption peaks at 294 and 257 nm, respectively. The intensities of these peaks, observed at 270 and 294 nm, increased proportionally with IOP elevation, reaching a threshold of 22 mmHg, which indicates the initiation of combination therapy.

For practical IOP-lowering applications, the AP-TSCL system also supports programmable therapy, offering alternative solutions for cases requiring multibolus regimens. The programmable release of various medications at distinct IOP stages (22 and 26 mmHg), mimicking the multibolus administration typical in conventional glaucoma treatment, is achieved through the integration of two different microfluidic designs (0.5 and 0.7 mm) into the AP-TSCL (Fig. 5D). This approach allows for timely and automatic escalation to more aggressive treatments when prior therapies fail to sufficiently lower IOP.

The AP-TSCL with two specific microfluidic designs (0.5 and 0.7 mm) initiated the release of additional medication (antiglaucoma drug II, brimonidine) as the IOP persisted in escalating and reached 26 mmHg, preventing the progression of glaucoma to a more severe state by halting an uncontrolled elevation in IOP (Fig. 5E). The overall theranostic performance was demonstrated (movie S5). This was further validated by UV-Vis spectrophotometry (Fig. 5F): The 247-nm brimonidine peak varied directly with the imposed IOP ramp to 26 mmHg. These proof-of-concept results confirm the feasibility of programmable therapy, enhancing the practical utility of AP-TSCL. Future work may incorporate additional dosing regions by integrating multiple microfluidic elements with distinct activation thresholds into the AP-TSCL to extend the therapeutic operating range. For example, additional thresholds could be implemented to address higher IOP ranges, such as 40 to 50 mmHg, that may occur during acute exacerbations (*36*).

In addition to evaluating on-demand release performance, we examined the chemical stability of timolol in the AP-TSCL device under ambient storage conditions. UV-Vis absorbance spectra collected weekly over a 5-week period consistently exhibited a strong peak at around 293 nm, characteristic of intact timolol molecules (fig. S37). No spectral shifts or degradation by-products were observed, indicating the preserved molecular structure throughout the storage duration. These findings confirm that the microfluidic drug reservoir and surrounding polymeric environment provide a chemically stable enclosure for the drug. Such long-term stability is critical for enabling preloaded, ready-to-use theranostic lenses that do not require frequent drug refilling or refrigeration. This result supports the potential for AP-TSCLs to be deployed as shelf-stable therapeutic devices suitable for both routine clinical use and at-home glaucoma management.

Ex vivo validation of the AP-TSCL on an enucleated bovine eye

We further evaluated the theranostic performance of the AP-TSCL ex vivo using an enucleated bovine eye, chosen for its structural similarity to the human eye. The ex vivo validation setup used a dual-needle cannulation technique applied to the bovine eye (fig. S38A). The first needle was connected to a syringe pump, enabling precise control of IOP by regulating the infusion and withdrawal of saline solution in the anterior chamber. The second needle was attached to a pressure gauge for real-time IOP measurements, ensuring accurate calibration. The AP-TSCL was conformably affixed to the corneal surface of the bovine eye.

The AP-TSCL demonstrated sufficient transparency over the pupil area when worn on the bovine eye, without obstructing the field of vision. To visualize the microfluidic drug-eluting component in the AP-TSCL system, black and green dyes were used. The cyclic stability of the AP-TSCL in releasing medications across five IOP cycles ranged from 16 to 26 mmHg, which was consistent with our previous in vitro results (fig. S38B). We observed reversibility and

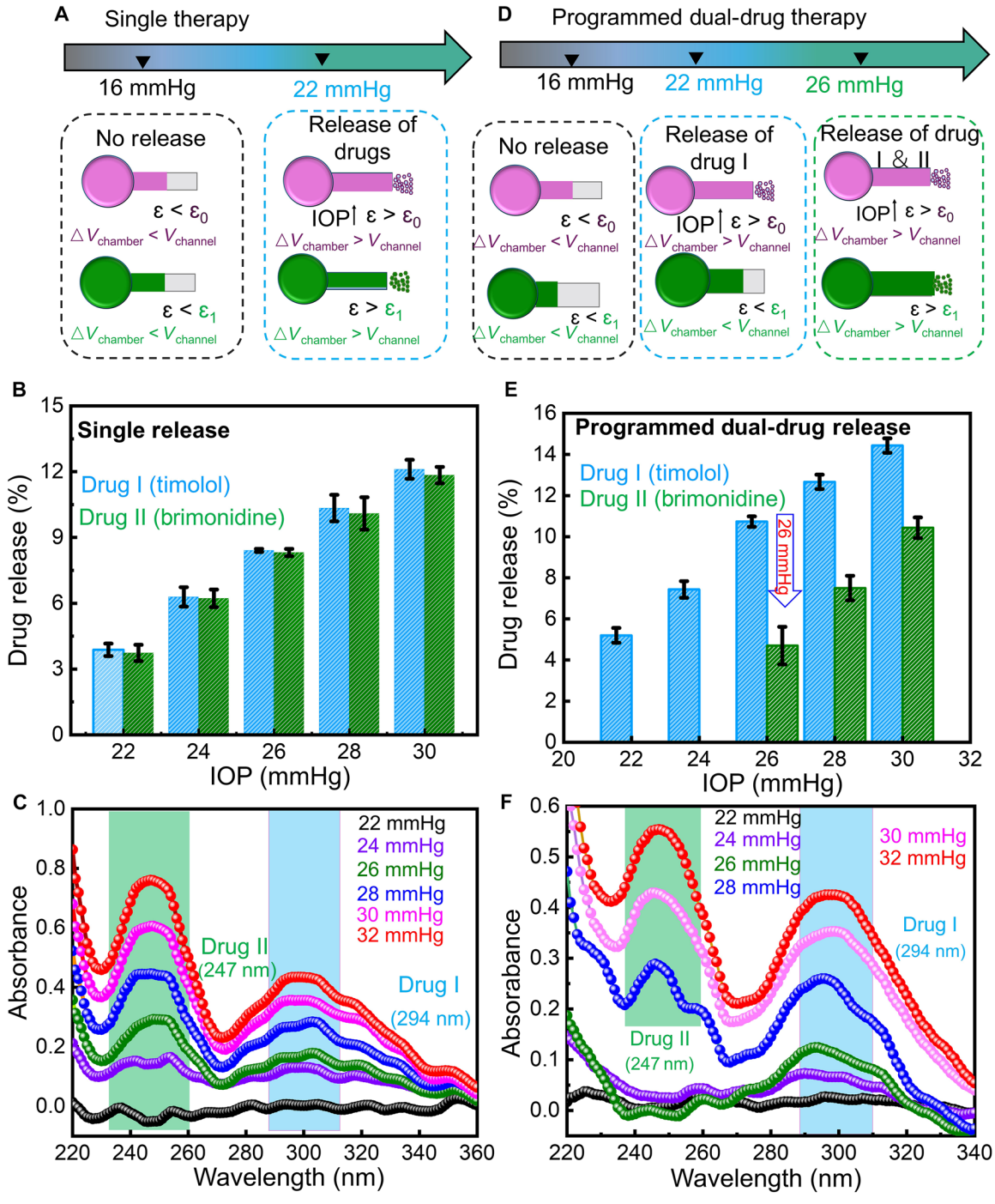

Fig. 5. Multimode IOP control enabled by the AP-TSCL, including single-stage combination release and programmed multistage release. (**A**) Schematic of the single IOP stage combination-release configuration, in which two identical microchannels (0.5 mm in width) are independently loaded with different medications (timolol and brimonidine) and actuated concurrently when the IOP exceeds the predefined threshold. (**B**) Drug release profiles measured under an elevated IOP (22 to 30 mmHg); blue and green bars denote release of drug I (timolol) and drug II (brimonidine), respectively. (**C**) UV-Vis spectra corresponding to dual-drug release, with blue and green shaded regions indicating medications I and II as the IOP increases from 22 to 32 mmHg. (**D**) Schematic of a staged-release configuration using microchannels with distinct geometries to enable sequential dosing, in which an initial medication (drug I) is released at the first IOP threshold, followed by a second medication (medication II) if the IOP remains elevated, reflecting stepwise clinical treatment strategies. (**E**) Representative programmed dual-drug release profile. (**F**) UV-Vis spectra of released medication collected at the designed release pressures, with medication I released at 22 mmHg (blue) and medication II at 26 mmHg (green). Values are presented as means ± SD; *n* values are indicated in the panels.

stability of the AP-TSCL's on-demand drug release capabilities during cyclic testing, highlighting precise controlled release in response to IOP changes (below or above 22 mmHg) (movie S6).

We also characterized the IOP sensing performance of the AP-TSCL ex vivo (fig. S38C). The system exhibited an increase in displacement with rising IOP, showing high sensitivity of ~0.06 mm/mmHg and strong linearity ($R^2 = 0.97$) in the 16- to 28-mmHg range. Overall, the AP-TSCL system demonstrates competitive theranostic performance among existing SCLs (table S3). The AP-TSCL uses a one-way, IOP-triggered release mechanism: When IOP exceeds a specific threshold, reservoir strain drives outward flow that opposes tear ingress. Antibackflow features, including narrowed outlets (capillary resistance), curved (or elongated) paths, and hydrophobic parylene coatings, further deter reflux.

Cytotoxicity and in vivo evaluation in rabbit eyes

To assess the biocompatibility of the AP-TSCL, time-dependent cytotoxicity assays were performed using human corneal epithelial cells (HCEpiCs). Cells were cultured at 37.5°C in contact with the AP-TSCL for up to 72 hours. Cell viability was quantified using the Cell Counting Kit-8 (CCK-8) assay. Fluorescence microscopy imaging revealed high cell viability, with live cells stained green and dead cells stained red (fig. S39A). Quantitative results indicated that viability remained above 98% in the AP-TSCL group, with no statistically significant difference compared to the negative control group ($n = 3$, $P > 0.05$), demonstrating cellular tolerance (fig. S39B). Flow cytometry analysis of apoptosis (fig. S39C) further confirmed the absence of substantial apoptotic response in the AP-TSCL group, supporting the cytocompatibility of the material. Fluorescein sodium staining was used to examine corneal surface integrity, with untreated corneas and a positive control condition (epithelial layer removal) included for comparison (fig. S39D). Representative images illustrate the staining patterns observed across groups. Corneal tissue morphology was further evaluated by hematoxylin and eosin (H&E) staining, which was used to assess epithelial and stromal architecture after lens wear relative to untreated controls (fig. S39E).

To further confirm the cytocompatibility of the AP-TSCL across diverse cell types, we extended the evaluation to two widely accepted models used in toxicity screening: human umbilical cord endothelial cells (HUVECs) and mouse fibroblast cells (L929). Both cell lines were cultured on the AP-TSCL surface for 72 hours at 37.5°C and assessed using CCK-8 viability assays. Consistent with results from HCEpiCs, viability remained above 97%, with no statistically significant difference from negative controls ($n = 3$, $P > 0.05$; fig. S40, A and B). Flow cytometry analysis confirmed minimal apoptosis (fig. S40C), and additional in vivo fluorescein staining and histological analysis revealed no corneal staining or epithelial damage after 14 days of AP-TSCL wear, and the corneal morphology remained consistent with that of the control group (fig. S40, D to E, and fig. S41). The results of H&E staining showed that, after 14 days of AP-TSCL wear, either without drug loading, or with single-drug or dual-drug loading, the rabbit corneas remained comparable to those of the untreated control group, with no signs of inflammation observed.

In vivo IOP monitoring and control of the AP-TSCL

To evaluate the biocompatibility, safety, and therapeutic efficacy of the AP-TSCL system, we conducted in vivo studies in New Zealand rabbit models of ocular hypertension. The AP-TSCL was applied directly to the rabbit eye, and glaucoma was induced by anterior chamber paracentesis at the temporal limbus, followed by slow injection of a compound carbomer solution into the anterior chamber, leading to elevated IOP compared with healthy controls (Fig. 6A). Two distinct models were established, a moderate hypertension model (IOP > 25 mmHg) and a severe hypertension model (IOP > 40 mmHg).

To assess IOP monitoring performance, the AP-TSCL was worn on anesthetized rabbit eyes, and deformation-induced liquid displacement in the microfluidic channels was used to estimate IOP in real time. Displacement readings exhibited a strong linear correlation with tonometer-based IOP measurements across a wide physiological range (15 to 55 mmHg, $R^2 > 0.97$, $P < 0.0001$; Fig. 6B), and this correlation was validated in side-by-side comparisons with commercial tonometers (fig. S42). Monitoring every 5 min over a 30-min period demonstrated high consistency and reproducibility with tonometry (Fig. 6C).

In a moderate hypertension model, the application of the AP-TSCL-Timo (loaded with timolol) produced a decrease in IOP, from ~25 mmHg to below 20 mmHg on day 1 (Fig. 6D), whereas untreated eyes remained hypertensive. This reduction was not significantly different ($P > 0.05$) from the effect achieved by topical timolol eye drops, confirming the AP-TSCL's therapeutic efficacy. The effect persisted over a 2-week regimen in which the lens was applied every other day for 30 min per session (seven total applications), demonstrating stable long-term IOP control (Fig. 6E). Over the 30-min monitoring window, AP-TSCL-Timo reduced the IOP from about 24 mmHg to below 20 mmHg, comparable to the topical timolol eye drop group, whereas untreated controls remained hypertensive. The AP-TSCL IOP sensor enabled real-time tracking of therapeutic response over a 30-min period immediately after lens application (defined as time 0) (Fig. 6F and fig. S43). AP-TSCL-Timo reduced the IOP from a high near 24 mmHg to below 20 mmHg in 30 min, comparable to the topical timolol eye drop group, whereas the untreated controls remained elevated. The device-based IOP readings were confirmed by tonometry at times 0 min (immediately after lens placement) and 30 min. During cyclic intracameral microbead injections that elevated IOP above 25 mmHg, IOP was allowed to return toward baseline before the next injection, yielding ~30-min challenge-recovery cycles (Fig. 6G), consistent with IOP-responsive drug delivery. Over 1 week of use, the AP-TSCL-Timo system matched the efficacy of commercial timolol eye drops (Fig. 6H and fig. S44).

In a severe ocular hypertension (SOH) model (IOP > 40 mmHg), we evaluated a dual-drug lens (AP-TSCL-Pro; timolol and brimonidine) against AP-TSCL-Timo, topical timolol drops, dual eye drops containing timolol and brimonidine, and untreated controls. AP-TSCL-Pro was compared with AP-TSCL-Timo, topical timolol drops, topical dual drops (timolol and brimonidine), and untreated controls. For the topical groups, drops were administered at time 0, immediately before the 30-min monitoring window, to align with the timing of lens placement in the TSCL groups. AP-TSCL-Pro elicited greater IOP reductions than AP-TSCL-Timo, topical timolol monotherapy, or no treatment ($P < 0.0001$), and its effect was comparable to that of combined topical timolol/brimonidine administration ($P > 0.05$) (Fig. 6I and fig. S45). To visualize in vivo dosing, rhodamine B and fluorescein isothiocyanate (FITC) were coloaded as fluorescent surrogates for timolol and brimonidine. There was negligible dye release under normotensive or blinking conditions, with distinct, simultaneous liberation of both fluorophores only upon IOP elevation, demonstrating IOP-triggered dual-drug delivery (fig. S46). We

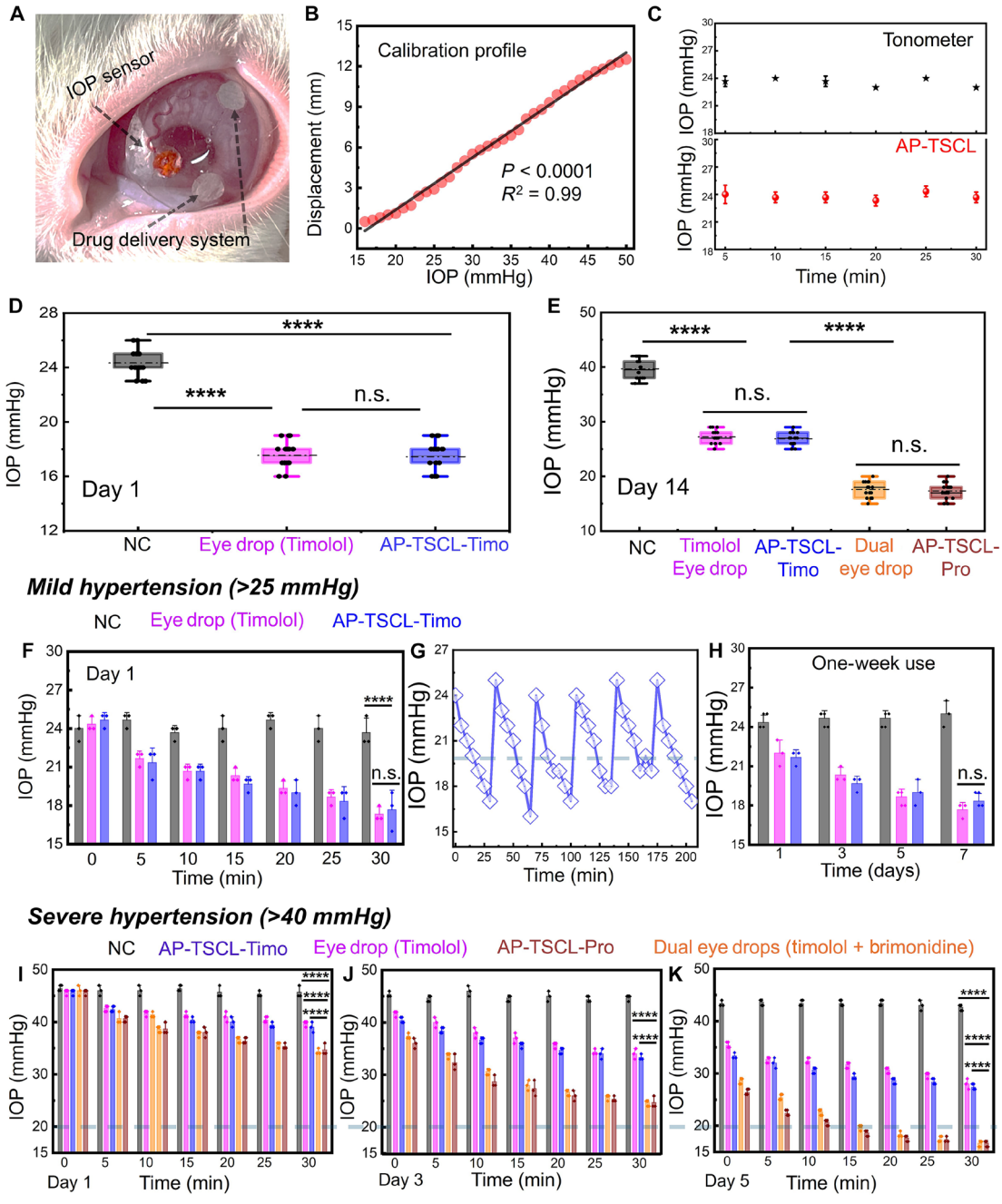

Fig. 6. In vivo IOP monitoring and therapeutic control using the AP-TSCL. (**A**) Photograph of the AP-TSCL placed on a rabbit eye. (**B**) Correlation between liquid-interface displacement measured by the AP-TSCL and IOP measured by tonometry [$n = 35$ paired measurements; $P < 0.0001$; $R^2 = 0.99$; best fit: $y = 0.38812x - 6.39664$; 95% confidence interval (CI) for the slope, 0.3784 to 0.39785; 95% CI for the intercept, −6.73226 to −6.06102]. (**C**) Comparison of AP-TSCL–derived IOP values with tonometer readings ($n = 3$). (**D**) IOP was measured on day 14 after timolol delivery by AP-TSCL versus untreated control in a mild ocular hypertension model (baseline IOP > 25 mmHg). NC, negative control (untreated); PC, positive control (topical standard-of-care drops, as indicated). Data are means ± SD (AP-TSCL-Timo: $N = 3$ rabbits, $n = 18$ measurements; AP-TSCL-Pro: $N = 3$ rabbits, $n = 18$ measurements; untreated control: $N = 3$ rabbits, $n = 18$ measurements; six measurements per rabbit). (**E**) IOP measurement by using the AP-TSCL microfluidic sensor after 2 weeks of treatment with AP-TSCL-Timo and AP-TSCL-Pro versus untreated control in an SOH model (IOP > 40 mmHg). Data are means ± SD ($N = 3$ rabbits per group; $n = 18$ measurements per group, six measurements per rabbit). (**F**) Representative real-time IOP monitoring and control over 30 min in a mild hypertension glaucoma model (baseline IOP > 25 mmHg); tonometer readings were used as the reference at times 0 and 30 min (red stars). For the topical timolol group, a single drop was instilled at time 0 immediately before initiating the 30-min monitoring period. Data are shown as means ± SD ($n = 3$). Statistics were analyzed by two-way repeated-measures ANOVA (time × treatment). (**G**) IOP-lowering performance of AP-TSCL-Timo across repeated IOP elevation cycles induced by methylcellulose (MC) injection over 200 min, with a baseline IOP of ~25 mmHg. (**H**) IOP over 1 week after timolol delivery by AP-TSCL versus untreated control in a mild ocular hypertension model (IOP > 25 mmHg). Data are shown as means ± SD ($n = 3$). Statistics were analyzed by two-way repeated-measures ANOVA (time × treatment). (**I** to **K**) Longitudinal IOP monitoring and control with AP-TSCL-Timo and AP-TSCL-Pro on day 1 (I), day 3 (J), and day 5 (K) in a severe hypertension model (IOP > 40 mmHg). Data are shown as means ± SD ($n = 3$). Statistics were analyzed by two-way repeated-measures ANOVA (time × treatment).

further examined 24-hour IOP regulation in rabbits fitted with the AP-TSCL (fig. S47). Over a full day, IOP was measured every 2 hours ($n = 3$) with an iCare TonoVet Plus in animals wearing the AP-TSCL versus untreated controls. The treated group maintained a stable, physiologically safe IOP throughout both light and dark cycles without any diurnal spikes. By contrast, the control group showed a consistently elevated IOP. These proof-of-concept results suggest AP-TSCL's ability to deliver around-the-clock IOP control, meeting the clinical demand for uninterrupted glaucoma management.

Over a 5-day treatment regimen, treatment was administered on alternating days, with the AP-TSCL applied on days 1, 3, and 5 (one session per treatment day) and no lens wear on days 2 and 4 (Fig. 6J). For the topical comparator groups, eye drops were administered on the same treatment days to match the dosing schedule. AP-TSCL-Pro achieved a substantial IOP reduction on day 1. By day 3, although IOP remained elevated, dual therapy (AP-TSCL-Pro) produced a greater reduction than monotherapy, including AP-TSCL-Timo and topical timolol eye drops [two-way repeated-measures analysis of variance (ANOVA) with post hoc multiple-comparisons correction; adjusted $P < 0.0001$ for comparisons between AP-TSCL-Pro and AP-TSCL-Timo and between AP-TSCL-Pro and topical timolol]. By day 5, the IOP was reduced to below 20 mmHg in the AP-TSCL-Pro group and remained stable for the remainder of the 2-week observation period, with a significantly lower IOP than those in the AP-TSCL-Timo, topical timolol, and untreated control groups (adjusted $P < 0.0001$ for all comparisons). Analysis of residual drug concentrations in the AP-TSCL microreservoirs remained well above therapeutic thresholds on days 1, 3, 5, and 7 in both moderate and severe hypertension models, indicating durable drug retention in the AP-TSCL with minimal depletion over time (fig. S48, A and B). In addition, after 12 hours of continuous wear, mimicking typical daily usage conditions, drug concentrations in the reservoirs remained unchanged (fig. S48, C and D), confirming the system's capacity for stable drug delivery over at least a 1-week period. IOP values recorded by the AP-TSCL sensor were found to closely align with those obtained from a commercial tonometer (Fig. 6, B and C), validating the accuracy and reliability of the mechanochromic sensing mechanism under physiological conditions.

To evaluate neuroprotective outcomes, we performed immunohistochemical (IHC) staining for glial fibrillary acidic protein (GFAP), brain-derived neurotrophic factor (BDNF), and Brn3a. In the standard glaucoma model, untreated eyes exhibited elevated GFAP, a marker of retinal gliosis and damage. In contrast, GFAP expression levels in AP-TSCL–treated eyes (timolol-loaded) were comparable to those in the control and eye drop groups (fig. S49). Meanwhile, markers of retinal ganglion cell survival, BDNF and Brn3a, were preserved in both the AP-TSCL and timolol drop groups. In the SOH model, GFAP remained high in the untreated group and both monotherapy groups. However, the dual-drug treatment (through AP-TSCL or drops) groups had less GFAP expression and maintained high expression of BDNF and Brn3a. These results underscore the benefit of combination therapy and support that AP-TSCL offers therapeutic efficacy equivalent to conventional eye drops while providing the added advantages of targeted, IOP-triggered, and programmable drug delivery.

DISCUSSION

We present an AP-TSCL platform that integrates a microfluidic sensor for noninvasive IOP monitoring with a multistage drug-eluting system for autonomous IOP management. This electronic- and power-free device combines softness, optical transparency, biocompatibility, and cost-effectiveness, offering a noninvasive approach to continuously monitor IOP and deliver individualized therapy. By coupling IOP readout with pressure-gated drug release, the platform is designed to enhance therapeutic efficacy while reducing unnecessary exposure under normotensive conditions, which may help mitigate ocular irritation and systemic side effects associated with conventional topical β-blockers in susceptible patients. In the broader context of IOP-responsive ocular devices, prior SCL strategies span electronic platforms with wireless sensing/actuation as well as mechanically actuated microfluidic valves or reservoirs that modulate flow under pressure. In this landscape, the AP-TSCL provides a complementary approach that achieves sensing-therapy integration without rigid electronics, supporting wearability and scalable manufacturing. Beyond glaucoma, the platform is compatible with commercial soft contact lenses and can be reconfigured to monitor additional tear biomarkers, enabling a wider range of ocular care applications.

These capabilities address several unmet needs in glaucoma management. IOP is dynamic and can exhibit diurnal and episodic fluctuations that are not fully captured by sporadic clinic-based measurements, whereas topical eye drops remain limited by variable adherence, tear washout, and nonuniform dosing exposure. Procedural interventions, including laser treatment or surgery, and sustained-release depots or implants can reduce reliance on daily eye drops but introduce trade-offs in invasiveness, reversibility, titratability, and patient-to-patient variability. In this therapeutic landscape, a wearable platform that can both track IOP trends and deliver medication in an event-responsive manner offers a complementary path toward individualized control, particularly for scenarios where hypertensive episodes may warrant dosing, whereas baseline periods may not.

Drug stability in the device and unintended leakage are central translational considerations for microreservoir-based ocular delivery, particularly for water-soluble agents such as timolol and brimonidine. Here, multiple lines of evidence support robust payload retention and minimal nontriggered release, including low passive leakage under tear-mimicking conditions and preservation of residual drug content in retrieved lenses over clinically relevant use windows. Together with barrier-coating strategies that mitigate diffusion-driven loss during storage and handling, these results support the feasibility of maintaining a stable on-device drug supply while limiting inadvertent dosing. From a safety standpoint, although timolol is a widely used first-line antiglaucoma therapy, topical β-blockers can be associated with ocular irritation and systemic side effects in susceptible patients. The AP-TSCL's pressure-gated, on-demand dosing is designed to preferentially deliver drug during hypertensive episodes, offering a path to preserve efficacy while potentially reducing unnecessary exposure under normotensive conditions.

More broadly, prior IOP-responsive and SCL approaches span electronic platforms with wireless sensing/actuation as well as mechanically actuated microfluidic valves or reservoirs that modulate flow under pressure. In this landscape, the AP-TSCL integrates a battery-free mechanofluidic IOP readout with a geometry-encoded, threshold-like release mechanism that couples sensing to therapy without rigid electronics, enabling selective dosing at an elevated IOP while preserving optical transparency and wearability. This design positions the AP-TSCL as a complementary strategy to existing electronic and microfluidic lenses, with a particular emphasis on simplicity, passive operation, and scalable manufacturability.

Although this theranostic lens exhibits promising features, opportunities remain to further improve IOP recording and IOP-responsive treatment. (i) Enhancing drug-loading capacity is a key area for extension of use time. Incorporating additional drug carriers, such as microchambers, or alternative reservoir geometries, such as ring-structured designs, could increase payload volume and support longer-duration therapy. We also explored the feasibility of refilling the AP-TSCL through needle injection (fig. S50). (ii) Long-term repeat-release systems can exhibit progressive depletion and declining dose output. To address this, we preloaded active compounds in a BASS matrix that serves as a solid-phase reservoir, enabling reestablishment of a saturated solution after each release event to support more consistent dosing. Preliminary results (fig. S51) showed stable drug output across multiple IOP-triggered cycles. In parallel, drug stability and unintended leakage remain critical translational considerations; ongoing optimization of barrier layers, reservoir sealing, and storage protocols will further strengthen payload retention and minimize passive release during handling and wear.

By addressing these opportunities and incorporating additional features for user convenience, long-term stability, scalable manufacturing, and cost-effectiveness, we envision an all-in-one theranostic wearable ocular device that provides insights into visual health and facilitates timely medical intervention in the prevention and management of glaucoma and other chronic diseases. This power- and electronic-free SCL represents a remarkable advancement toward multifunctional ocular medical devices that integrate diagnostics and therapeutics for intelligent ocular health care delivery. It lays the groundwork for developing a family of pharmacy-on-a-contact-lens tools capable of delivering clinically relevant information about human health and establishes the foundation for next-generation, self-powered, electronic-free SCLs capable of accessible diagnosis and therapeutics.

MATERIALS AND METHODS

Study design

This study developed a battery- and electronics-free AP-TSCL and evaluated its performance for real-time, noninvasive IOP monitoring and IOP-triggered drug delivery. We tested the device on an artificial eye (in vitro), enucleated bovine eyes (ex vivo), and New Zealand White rabbits (in vivo) and benchmarked IOP readings against a commercial tonometer. No formal power analysis was performed; sample sizes were determined a priori based on feasibility and the prior literature, with per-experiment n and technical/biological replicates reported in the figure legends and in this section. Prespecified end points were (i) IOP tracking accuracy within 19 to 40 mmHg and (ii) pressure-activated release above a predefined threshold; data collection stopped when these end points were met. Inclusion criteria were intact corneas and stable baseline IOP; samples with visible damage/leakage or instrumentation failure were excluded according to prespecified criteria. For animal experiments, rabbits were assigned to treatment/control conditions using a random number generator; cage location and handling were balanced across groups. Tonometer readings, image analyses, and histology scoring were performed by investigators blinded to group allocation; allocation was concealed until primary analyses were complete. Each experiment included $\geq$3 biological replicates with $\geq$3 technical replicates per condition (exact n for each panel provided in figure legends). Independent repeats were performed on separate days to verify reproducibility. All in vivo experiments adhered to the ARVO guidelines for the use of animals in ophthalmic and vision research and were approved by the Institutional Animal Care and Use Committee of Sun Yat-Sen University (SYSU-IACUC-2024-002423).

Statistical analysis

Statistical analyses were performed in MATLAB (R2018a; MathWorks). Unless otherwise noted in the figure legends, data are presented as means ± SD. Normality was assessed using the Shapiro-Wilk test. When data did not meet normality assumptions, nonparametric tests were applied (Mann-Whitney U test for two-group comparisons and Kruskal-Wallis test for multiple-group comparisons), with appropriate post hoc corrections where applicable. Two-group comparisons were performed using unpaired, two-tailed Student's t tests with Welch's correction, and comparisons among multiple groups were performed using one-way ANOVA followed by Tukey's post hoc test. For longitudinal measurements with repeated observations from the same animals over time, two-way repeated-measures ANOVA was used, followed by post hoc multiple-comparisons correction where appropriate, as specified in the corresponding figure legends. Statistical significance was defined as $^{*}P < 0.05$, $^{**}P < 0.01$, $^{***}P < 0.001$, and $^{****}P < 0.0001$; n.s., not significant. The number of independent experiments (n) is indicated in the corresponding figure legends. All individual-level data are available in data file S1.

Supplementary Materials

The PDF file includes:

Materials and Methods
Figs. S1 to S51
Tables S1 to S3
Legend for data file S1
Legends for movies S1 to S6
References (*37*–*49*)

Other Supplementary Material for this manuscript includes the following:

Data file S1
Movies S1 to S6
MDAR Reproducibility Checklist

REFERENCES AND NOTES

1. A. Sheybani, R. Scott, T. W. Samuelson, M. Y. Kahook, D. I. Bettis, I. I. K. Ahmed, J. D. Stephens, D. Kent, T. J. Ferguson, L. W. Herndon, Open-angle glaucoma: Burden of illness, current therapies, and the management of nocturnal IOP variation. *Ophthalmol. Therapy* **9**, 1–14 (2020).
2. Y. Shaikh, F. Yu, A. L. Coleman, Burden of undetected and untreated glaucoma in the United States. *Am. J. Ophthalmol.* **158**, 1121–1129.e1 (2014).
3. R. Shean, N. Yu, S. Guntipally, V. Nguyen, X. He, S. Duan, K. Gokoffski, Y. Zhu, B. Xu, Advances and challenges in wearable glaucoma diagnostics and therapeutics. *Bioengineering* **11**, 138 (2024).
4. L. P. Cohen, L. R. Pasquale, Clinical characteristics and current treatment of glaucoma. *Cold Spring Harb. Perspect. Med.* **4**, a017236 (2014).
5. J. C. Morrison, E. C. Johnson, W. Cepurna, L. Jia, Understanding mechanisms of pressure-induced optic nerve damage. *Prog. Retin. Eye Res.* **24**, 217–240 (2005).
6. M. O. Gordon, J. A. Beiser, J. D. Brandt, D. K. Heuer, E. J. Higginbotham, C. A. Johnson, J. L. Keltner, J. P. Miller, R. K. Parrish II, M. R. Wilson, M. A. Kass, The ocular hypertension treatment study: Baseline factors that predict the onset of primary open-angle glaucoma. *Arch. Ophthalmol.* **120**, 714–720 (2002).
7. M. A. Kass, D. K. Heuer, E. J. Higginbotham, C. A. Johnson, J. L. Keltner, J. P. Miller, R. K. Parrish II, M. R. W. , M. O. Gordon, The ocular hypertension treatment study: A randomized trial determines that topical ocular hypotensive medication delays or prevents the onset of primary open-angle glaucoma. *Arch. Ophthalmol.* **120**, 701–713 (2002).
8. D. R. Anderson, Collaborative normal tension glaucoma study. *Curr. Opin. Ophthalmol.* **14**, 86–90 (2003).
9. J. Bader, M. Zeppieri, S. J. Havens, "Tonometry" in *StatPearls* (StatPearls Publishing LLC, 2023).
10. T. Y. Kim, J. W. Mok, S. H. Hong, S. H. Jeong, H. Choi, S. Shin, C.-K. Joo, S. K. Hahn, Wireless theranostic smart contact lens for monitoring and control of intraocular pressure in glaucoma. *Nat. Commun.* **13**, 6801 (2022).

11. P. Vitish-Sharma, A. G. Acheson, R. Stead, J. Sharp, A. Abbas, M. Hovan, C. Maxwell-Armstrong, B. Guo, A. J. King, Can the SENSIMED Triggerfish® lens data be used as an accurate measure of intraocular pressure? *Acta Ophthalmol.* **96**, e242–e246 (2018).
12. A. Belamkar, A. Harris, R. Zukerman, B. Siesky, F. Oddone, A. Verticchio Vercellin, T. A. Ciulla, Sustained release glaucoma therapies: Novel modalities for overcoming key treatment barriers associated with topical medications. *Ann. Med.* **54**, 343–358 (2022).
13. A. Farkouh, P. Frigo, M. Czejka, Systemic side effects of eye drops: A pharmacokinetic perspective. *Clin. Ophthalmol.* **10**, 2433–2441 (2016).
14. B. L. Nordstrom, D. S. Friedman, E. Mozaffari, H. A. Quigley, A. M. Walker, Persistence and adherence with topical glaucoma therapy. *Am. J. Ophthalmol.* **140**, 598–606 (2005).
15. A. L. Robin, D. Covert, Does adjunctive glaucoma therapy affect adherence to the initial primary therapy? *Ophthalmology* **112**, 863–868 (2005).
16. G. Montesano, G. Ometto, I. I. K. Ahmed, P. Y. Ramulu, D. F. Chang, D. P. Crabb, G. Gazzard, Five-year visual field outcomes of the HORIZON trial. *Am. J. Ophthalmol.* **251**, 143–155 (2023).
17. Y. Zhu, S. Li, J. Li, N. Falcone, Q. Cui, S. Shah, M. C. Hartel, N. Yu, P. Young, N. R. de Barros, Z. Wu, R. Haghniaz, M. Ermis, C. Wang, H. Kang, J. Lee, S. Karamikamkar, S. Ahadian, V. Jucaud, M. R. Dokmeci, H.-J. Kim, A. Khademhosseini, Lab-on-a-contact lens: Recent advances and future opportunities in diagnostics and therapeutics. *Adv. Mater.* **34**, 2108389 (2022).
18. C. Yang, Q. Wu, J. Liu, J. Mo, X. Li, C. Yang, Z. Liu, J. Yang, L. Jiang, W. Chen, H.-j. Chen, J. Wang, X. Xie, Intelligent wireless theranostic contact lens for electrical sensing and regulation of intraocular pressure. *Nat. Commun.* **13**, 2556 (2022).
19. H. Seo, W. G. Chung, Y. W. Kwon, S. Kim, Y.-M. Hong, W. Park, E. Kim, J. Lee, S. Lee, M. Kim, K. Lim, I. Jeong, H. Song, J.-U. Park, Smart contact lenses as wearable ophthalmic devices for disease monitoring and health management. *Chem. Rev.* **123**, 11488–11558 (2023).
20. Y. Zhu, R. Nasiri, E. Davoodi, S. Zhang, S. Saha, M. Linn, L. Jiang, R. Haghniaz, M. C. Hartel, V. Jucaud, M. R. Dokmeci, A. Herland, E. Toyserkani, A. Khademhosseini, A microfluidic contact lens to address contact lens-induced dry eye. *Small* **19**, 2207017 (2023).
21. S. Li, Y. Zhu, R. Haghniaz, S. Kawakita, S. Guan, J. Chen, Z. Li, K. Mandal, J. Bahari, S. Shah, J. Guo, H. Kang, W. Sun, H.-J. Kim, V. Jucaud, M. R. Dokmeci, P. Kollbaum, C. H. Lee, A. Khademhosseini, A microchambers containing contact lens for the noninvasive detection of tear exosomes. *Adv. Funct. Mater.* **32**, 2206620 (2022).
22. M. S. Sridhar, Anatomy of cornea and ocular surface. *Indian J. Ophthalmol.* **66**, 190–194 (2018).
23. N. Adrus, M. A. bin M. Farizal, J. Jamaluddin, F. S. bin Syaiful Azim, F. M. Mizi, S. N. Kumar, J. J. Govindasamy, *Contact Lenses* (Springer, 2025).
24. E. Khanjani, A. Fergola, J. A. López Martínez, S. Nazarnezhad, J. Casals Terre, S. L. Marasso, B. Aghajanloo, Capillary microfluidics for diagnostic applications: Fundamentals, mechanisms, and capillarics. *Lab Chip Technol.* **4**, 1502127 (2025).
25. P. Kolliopoulos, S. Kumar, Capillary flow of liquids in open microchannels: Overview and recent advances. *NPJ Microgravity* **7**, 51 (2021).
26. R. Haghniaz, A. Gangrade, H. Montazerian, F. Zarei, M. Ermis, Z. Li, Y. Du, S. Khosravi, N. R. de Barros, K. Mandal, A. Rashad, F. Zehtabi, J. Li, M. R. Dokmeci, H.-J. Kim, A. Khademhosseini, Y. Zhu, An all-in-one transient theranostic platform for intelligent management of hemorrhage. *Adv. Sci.* **10**, e2301406 (2023).
27. C. Xu, Z. Wei, H. Gao, Y. Bai, H. Liu, H. Yang, Y. Lai, L. Yang, Bioinspired mechano-sensitive macroporous ceramic sponge for logical drug and cell delivery. *Adv. Sci.* **4**, 1600410 (2017).
28. C. Gonzalez-Obeso, E. J. Hartzell, R. A. Scheel, D. L. Kaplan, Delivering on the promise of recombinant silk-inspired proteins for drug delivery. *Adv. Drug Deliv. Rev.* **192**, 114622 (2023).
29. B. Bengtsson, A. Heijl, A long-term prospective study of risk factors for glaucomatous visual field loss in patients with ocular hypertension. *J. Glaucoma* **14**, 135–138 (2005).
30. M. B. Sultan, S. L. Mansberger, P. P. Lee, Understanding the importance of IOP variables in glaucoma: A systematic review. *Surv. Ophthalmol.* **54**, 643–662 (2009).
31. G. F. Schwartz, H. A. Quigley, Adherence and persistence with glaucoma therapy. *Surv. Ophthalmol.* **53**, S57–S68 (2008).
32. B. Sleath, S. Blalock, D. Covert, J. L. Stone, A. C. Skinner, K. Muir, A. L. Robin, The relationship between glaucoma medication adherence, eye drop technique, and visual field defect severity. *Ophthalmology* **118**, 2398–2402 (2011).
33. L. F. Valladales-Restrepo, M. C. Oyuela-Gutiérrez, A. C. Delgado-Araujo, J. E. Machado-Alba, Use pattern of ophthalmic antiglaucoma agents with and without preservatives: A cross-sectional study. *Pharmaceuticals (Basel)* **16**, 743 (2023).
34. C.-C. Peng, M. T. Burke, B. E. Carbia, C. Plummer, A. Chauhan, Extended drug delivery by contact lenses for glaucoma therapy. *J. Control. Release* **162**, 152–158 (2012).
35. J. Sun, Y. Lei, Z. Dai, X. Liu, T. Huang, J. Wu, Z. P. Xu, X. Sun, Sustained release of brimonidine from a new composite drug delivery system for treatment of glaucoma. *ACS Appl. Mater. Interfaces* **9**, 7990–7999 (2017).
36. D. Križaj, "What is glaucoma?" in *Webvision: The Organization of the Retina and Visual System [Internet]* (Univ. of Utah Health Sciences Center, 2019).
37. J. Zhang, K. Kim, H. J. Kim, D. Meyer, W. Park, S. A. Lee, Y. Dai, B. Kim, H. Moon, J. V. Shah, K. E. Harris, B. Collar, K. Liu, P. Irazoqui, H. Lee, S. A. Park, P. S. Kollbaum, B. W. Boudouris, C. H. Lee, Smart soft contact lenses for continuous 24-hour monitoring of intraocular pressure in glaucoma care. *Nat. Commun.* **13**, 5518 (2022).
38. Z. Du, G. Zhao, A. Wang, W. Sun, S. Mi, Pressure-triggered microfluidic contact lens for ocular drug delivery. *ACS Appl. Polym. Mater.* **4**, 7290–7299 (2022).
39. W. Yang, X. Zhang, Y. Wang, Q. Fan, S. Zhang, Y. Chen, X. Shen, M. Xie, X. Duan, Notched-ring structured microfluidic contact lens for intraocular pressure monitoring. *Appl. Phys. Lett.* **119**, 193701 (2021).
40. I. K. Karunaratne, C. H. C. Lee, P. W. Or, Y. Wei, I. T. Chong, Y. Yang, M. Yu, D. C. C. Lam, Wearable dual-element intraocular pressure contact lens sensor. *Sens. Actuators A Phys.* **321**, 112580 (2021).
41. J. Kim, J. Park, Y. G. Park, E. Cha, M. Ku, H. S. An, K. P. Lee, M. I. Huh, J. Kim, T. S. Kim, D. W. Kim, H. K. Kim, J. U. Park, A soft and transparent contact lens for the wireless quantitative monitoring of intraocular pressure. *Nat. Biomed. Eng.* **5**, 772–782 (2021).
42. J. B. Ciolino, C. F. Stefanescu, A. E. Ross, B. Salvador-Culla, P. Cortez, E. M. Ford, K. A. Wymbs, S. L. Sprague, D. R. Mascoop, S. S. Rudina, S. A. Trauger, F. Cade, D. S. Kohane, In vivo performance of a drug-eluting contact lens to treat glaucoma for a month. *Biomaterials* **35**, 432–439 (2014).
43. T. Y. Kim, S. Shin, H. Choi, S. H. Jeong, D. Myung, S. K. Hahn, Smart contact lenses with a transparent silver nanowire strain sensor for continuous intraocular pressure monitoring. *ACS Appl. Bio Mater.* **4**, 4532–4541 (2021).
44. Z. Liu, G. Wang, C. Ye, H. Sun, W. Pei, C. Wei, W. Dai, Z. Dou, Q. Sun, C. T. Lin, Y. Wang, H. Chen, G. Shen, An ultrasensitive contact lens sensor based on self-assembly graphene for continuous intraocular pressure monitoring. *Adv. Funct. Mater.* **31**, 2010991 (2021).
45. H. An, L. Chen, X. Liu, B. Zhao, H. Zhang, Z. Wu, Microfluidic contact lenses for unpowered, continuous and non-invasive intraocular pressure monitoring. *Sens. Actuators A Phys.* **295**, 177–187 (2019).
46. M. Yuan, Z. Liu, X. Wu, H. Gou, Y. Zhang, X. Ning, W. Li, Z. Yao, Y. Wang, W. Pei, H. Chen, High-sensitive microfluidic contact lens sensor for intraocular pressure visualized monitoring. *Sens. Actuators A Phys.* **354**, 114250 (2023).
47. X. Ding, G. Ben-Shlomo, L. Que, Soft contact lens with embedded microtubes for sustained and self-adaptive drug delivery for glaucoma treatment. *ACS Appl. Mater. Interfaces* **12**, 45789–45795 (2020).
48. J. Kim, M. Kim, M. S. Lee, K. Kim, S. Ji, Y. T. Kim, J. Park, K. Na, K. H. Bae, H. Kyun Kim, F. Bien, C. Young Lee, J. U. Park, Wearable smart sensor systems integrated on soft contact lenses for wireless ocular diagnostics. *Nat. Commun.* **8**, 14997 (2017).
49. J. Xu, Y. Ge, R. Bu, A. Zhang, S. Feng, J. Wang, J. Gou, T. Yin, H. He, Y. Zhang, X. Tang, Co-delivery of latanoprost and timolol from micelles-laden contact lenses for the treatment of glaucoma. *J. Control. Release* **305**, 18–28 (2019).

Acknowledgments

Funding: This work was supported by the Terasaki Institute for Biomedical Innovation Faculty Startup Fund to Y.Z. and the National Research Foundation of Korea (NRF) Nano & Material Technology Development Program (RS-2024-00416938) to T.-W.L., funded by the Ministry of Science and ICT. **Author contributions:** Y.Z. designed the overall project and experimental study. Y.Z. conceptualized the AP-TSCL device. Y.Z., Y.C., Y.D., and S.K. conducted experiments, including fabrication and characterizations of the AP-TSCL device. C.L. developed the AI-empowered computer vision for the autonomous IOP assessment. C.Z. and P.D. performed in vivo experiments. L.C. advised on and designed in vivo validations with glaucoma rabbit models. J.S.W. fabricated the contact lens mold and provided guidance on contact lens fabrication. R.H. performed the design and fabrication of the BASS. T.-W.L. contributed to the manuscript revision and preparation of the response. J.W. conducted the in vitro cytotoxicity test. Y.Z. wrote the manuscript with contributions from all authors. **Competing interests:** Y.Z. is an inventor on a patent application (PCT/US2025/021708) submitted by the Terasaki Institute for Biomedical Innovation, titled "Theranostic smart contact lens for monitoring pressure." The other authors declare that they have no competing interests. **Data, code, and materials availability:** All raw and processed data associated with this study are present in the paper or the Supplementary Materials and data file S1. A full code is publicly available on GitHub under the project "IOP-Microfluid-Tracking": https://github.com/ChenshuLiu/IOP-Microfluid-tracking.git. An immutable snapshot of the repository is archived on Zenodo (DOI: 10.5281/zenodo.17926949). All other materials are commercially available. Noncommercial, lab-fabricated components, such as AP-TSCL device prototypes, fabrication molds/masters, and related custom parts, are available from the corresponding author upon reasonable request and, where required, under a standard material transfer agreement.

Submitted 5 September 2024
Resubmitted 22 September 2025
Accepted 18 March 2026
Published 8 April 2026
10.1126/scitranslmed.ads9541

Science Translational Medicine

Real-time intraocular pressure monitoring and responsive drug release in preclinical models by an all-polymer smart contact lens

Yuting Cai, Chenguang Zhang, Pengrui Dang, Chenshu Liu, Yuxuan Du, Reihaneh Haghniaz, Jiechen Wang, Safoora Khosravi, Zhengtang Luo, Peyman Servati, Lili Chen, James S. Wolffsohn, Tae-Woo Lee, and Yangzhi Zhu

Sci. Transl. Med. **18** (844), eads9541. DOI: 10.1126/scitranslmed.ads9541

Editor's summary

Smart contact lenses have promise for the monitoring and treatment of conditions such as intraocular pressure changes in glaucoma. Many current smart lenses use electronic components that may compromise wearer comfort and safety. Here, Cai *et al.* designed a mechanically responsive, all-polymer contact lens system to detect changes in intraocular pressure and release one or more drugs at predetermined pressure thresholds. Their studies in ex vivo model eyes and in rabbits with ocular hypertension showed that the polymer lens reliably measured intraocular pressure compared with standard measurement tools and that the pressure-driven release of timolol or brimonidine provided a therapeutic effect similar to that of manually applied medicated eye drops. This preclinical study demonstrates that a simple mechanical mechanism has potential to provide on-demand drug delivery for glaucoma management. —Molly Ogle